Environmental Science & Technology

Article

pubs.acs.org/est

Roles of Radiolytic and Externally Generated H_2 in the Corrosion of Fractured Spent Nuclear Fuel

Nazhen Liu,[†] Linda Wu,[†] Zack Qin,[†] and David W. Shoesmith*[,†,‡]

[†]Department of Chemistry, The University of Western Ontario, London, Ontario N6A 5B7, Canada

[‡]Surface Science Western, The University of Western Ontario, London, Ontario N6G 0J3, Canada

Supporting Information

ABSTRACT: A 2-D model for the corrosion of spent nuclear fuel inside a failed nuclear waste container has been modified to determine the influence of various redox processes occurring within fractures in the fuel. The corrosion process is driven by reaction of the fuel with the dominant α radiolysis product, H_2O_2. A number of reactions are shown to moderate or suppress the corrosion rate, including H_2O_2 decomposition and a number of reactions involving dissolved H_2 produced either by α radiolysis or by the corrosion of the steel container vessel. Both sources of H_2 lead to the suppression of fuel corrosion, with their relative importance being determined by the radiation dose rate, the steel corrosion rate, and the dimensions of the fractures in the fuel. The combination of H_2 from these two sources can effectively prevent corrosion when only micromolar quantities of H_2 are present.

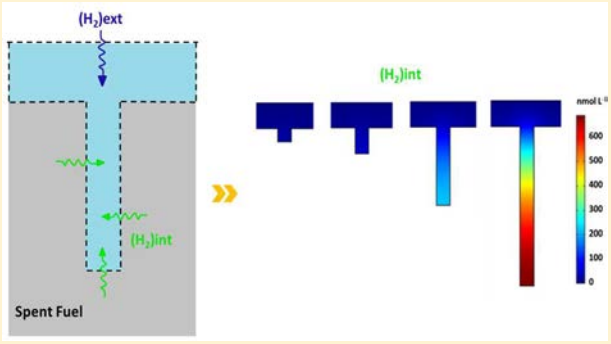

1. INTRODUCTION

If nuclear energy is to play an important role in alleviating the risk of global climate change, it must be demonstrated that the high-level waste can be safely disposed of. The recommended approach for the long-term management of used nuclear fuel in Canada is adaptive phased management.[1] The repository concept is based on multiple barriers including the fuel bundles, durable metal containers with an outer layer of copper and an inner carbon steel vessel, a clay buffer and seals around the container, and a deep geologic environment.[2,3] A key barrier in this sequence is the corrosion-resistant container that is expected to isolate the used fuel from the repository environment.[4−6] However, it is judicious to examine the consequences of container failure and the exposure of used fuel bundles to groundwater.

In the anoxic conditions anticipated in a deep geological repository, water radiolysis, resulting from the radiation fields associated with the used fuel, will be the only source of oxidants within a failed groundwater-containing container. The key radiolysis product, H_2O_2, has been shown to be the primary oxidant driving fuel corrosion.[7] Oxidation of fuel (U^{IV}) will produce the oxidized form (U^{VI}) with a considerably higher solubility than U^{IV}, leading to the release of radionuclides.[8] Another corrosion front, sustained by water reduction to produce the potential redox scavengers, Fe^{2+} and H_2, is present on the inner surface of the carbon steel vessel. It has also been shown that, under anaerobic groundwater conditions, metallic iron can reduce oxidized uranium.[9,10]

Dissolved H_2 has been shown to suppress fuel corrosion and radionuclide release in a number of investigations.[11−17] Broczkowski et al.[17] used electrochemical methods to show that this suppression could be attributed to the formation of reductive radicals by H_2 oxidation catalyzed on the noble metal (ε) particles present in SIMFUEL pellets, which act as galvanically coupled anodes within the fuel matrix. This catalytic effect was confirmed by Jonsson et al., who showed that during γ-irradiation, 1 bar H_2 was sufficient to inhibit UO_2 corrosion when 0.1 wt % Pd was present. In experiments conducted in an N_2 purged solution, 3 wt % Pd could prevent corrosion when only radiolytically produced H_2 was present.[18] Because at room temperature, the dissolved molecular H_2 is known to be chemically inert, these experiments confirm that the activation of H_2 by noble metals is a key mechanism in suppressing fuel oxidation.[15−18]

The development of radiolytic models for spent fuel corrosion has been reviewed.[19] A mixed potential model based on electrochemical parameters for fuel corrosion was developed.[20] This model consists of corrosion fronts on the fuel and steel vessel surfaces, interconnected by diffusion processes in the groundwater assumed to flood the container on failure. Jonsson et al. developed a comprehensive model that integrated the available kinetic data and tried to account for the geometrical distribution of the radiation dose rate at the surface of the fuel and the effects of the oxidant scavengers Fe^{2+} and H_2, fuel burn-up, and groundwater chemistry.[21] It was

Received: August 17, 2016
Revised: October 16, 2016
Accepted: October 16, 2016
Published: October 17, 2016

© 2016 American Chemical Society

DOI: 10.1021/acs.est.6b04167
Environ. Sci. Technol. 2016, 50, 12348−12355

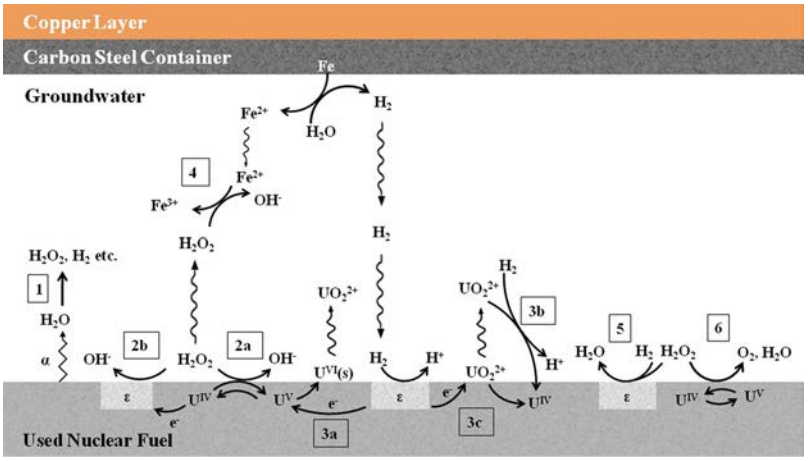

Figure 1. Schematic illustration of the reactions included in the model for the α-radiolytic corrosion of spent nuclear fuel.[22]

concluded that a H_2 partial pressure of only 0.1 bar would effectively inhibit the dissolution of the spent fuel (aged ≥100 years).

Using this database generated by Jonsson et al., Wu et al.[22] developed a 1-D model for fuel corrosion that includes a full α-radiolytic reaction set. This model was subsequently expanded to account for the complex geometry of spent fuel, particularly the fracturing of the fuel pellets due to the thermal stress during the in-reactor irradiation and the cooling process on discharge from reactor.[23] This 2-D model showed that both radiolytically produced H_2 ($(H_2)_{int}$) and H_2 from steel corrosion ($(H_2)_{ext}$) can inhibit fuel corrosion, although $(H_2)_{ext}$ would be expected to be the primary redox scavenger. However, the transport of $(H_2)_{ext}$ to the fuel surfaces deep within fractures will be limited, making it important to determine the role $(H_2)_{int}$ may play in suppressing fuel corrosion at these locations.

It is also judicious to examine the consequences of the absence of any $(H_2)_{ext}$, a scenario that is unlikely but could arise if the walls of the steel vessel become passivated.[24] Because separating the effects of $(H_2)_{int}$ and $(H_2)_{ext}$ experimentally would be difficult, if not impossible, we have used our model to separate them.

We have modified the published 2-D model to determine the separate effects of $(H_2)_{int}$ and $(H_2)_{ext}$ on the suppression of spent fuel corrosion for different fracture geometries, α-radiation dose rates, and concentration of external H_2. Our primary objective is to determine the relative importance of these two H_2 sources in determining the fuel corrosion rate and, hence, the radionuclide release rate inside a failed waste container.

2. MODEL DESCRIPTION

Under irradiation, the fuel undergoes a number of microstructural and compositional changes involving the formation of rare earth (RE^{III}) elements and noble metal (ε) particles, which have been shown to influence its chemical reactivity under anticipated disposal conditions.[25] The RE^{III} elements cause an increase in the electrical conductivity of the fuel matrix, and the noble metal particles, generally segregated to grain boundaries, can act as either cathodes or anodes (depending on the prevailing redox conditions in the exposure environment) galvanically coupled to the UO_2 matrix.

Figure 1 illustrates the two corrosion fronts within the container and the main reactions involved in controlling redox conditions and, hence, the process of fuel corrosion. The model includes the following reactions.

(1) The production of H_2O_2 and H_2 by water radiolysis. This approach considers only the radiolytic production of these two molecular species as opposed to a full radiolysis model that would include the radical species as well (e.g., OH, H, etc.). Our previous comparison of this simplified model to the full model showed the simplified model overestimates the steady-state $[UO_2^{2+}]$ by ~20% at the bottom of a fracture (width = 0.1 mm, depth =1 mm); i.e., it overestimates the oxidizing effect of H_2O_2 compared to the reducing effect of H_2, making our calculations in this paper conservative.[23]

(2) The oxidative dissolution (corrosion) of UO_2 supported by H_2O_2 reduction on both the UO_2 surface (reaction 2a)[26] and noble metal particles (reaction 2b).[18]

(3) The reduction of oxidized surface species (U^V and U^{VI}) by H_2 oxidation on noble metal particles (reaction 3a)[27] and of dissolved UO_2^{2+} either by reaction with H_2 in solution (reaction 3b)[28] or with H_2 catalyzed on the fuel surface (reaction 3c).[29]

(4) The scavenging of H_2O_2 in homogeneous solution by reaction with Fe^{2+}.[30]

(5) The reaction of H_2O_2 with H_2 catalyzed by noble metal particles.[31]

(6) The decomposition of H_2O_2 to O_2 and H_2O.[26]

The kinetic details of these reactions and their incorporation into the model have been described elsewhere.[22] Dissolution as UO_2^{2+} is assumed to be unimpeded by the formation on the dissolving surface of corrosion product deposits (e.g., $UO_3 2H_2O$), which could significantly influence the corrosion rate. This would be the case in groundwater containing sufficient HCO_3^- to completely complex and dissolve the UO_2^{2+} as $UO_2(HCO_3)_a^{2-a}$.

Figure 2 shows a cross-section of the fuel−solution interface illustrating the simplified geometry adopted to simulate radiolytic corrosion inside a fracture in a fuel pellet. Radiolysis is considered to occur uniformly within a thin layer of solution on the fuel surface with a thickness of 13 μm,[32] given by the average penetration distance of α-radiation in water.[33] Beyond this layer, no radiolysis products (H_2O_2, H_2 etc.) are produced. The boundary of the uniform radiation zone on the fuel surface is indicated by red dashed lines in Figure 2.This is a simplification because the dose rate will actually nonuniformly

DOI: 10.1021/acs.est.6b04167
Environ. Sci. Technol. 2016, 50, 12348−12355

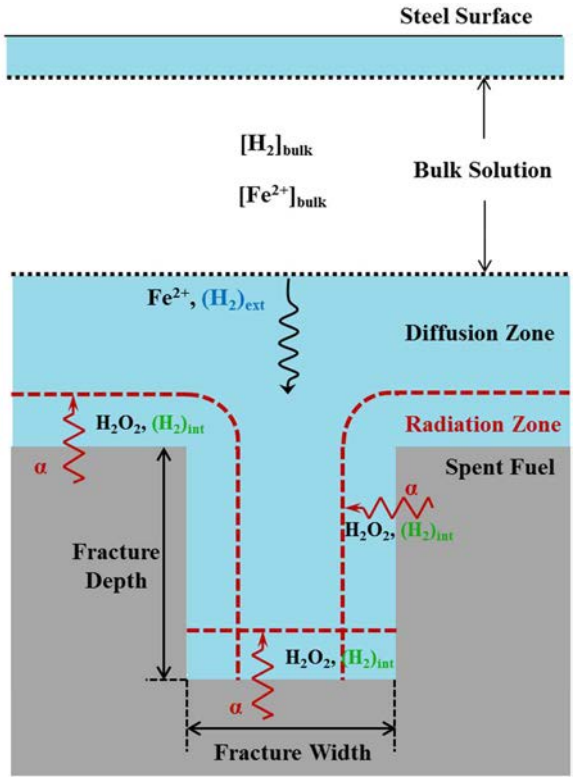

Figure 2. Model arrangement showing a cross-section of the fuel–solution interface for the simulation of radiolytic corrosion inside a fracture in a fuel pellet;[22] the area in light blue indicates the diffusion zone.

distributed, the α-particles losing energy along the penetration path. We have previously calculated the consequences of assuming a uniform energy distribution rather than the actual exponential dose distribution and showed the simplification has only a marginal effect on predicted corrosion rates.[32]

The diffusion zone (area indicated as light blue in Figure 2) is the H_2O layer on the fuel surface over which species can diffuse and beyond which uniform concentrations are presumed to prevail. The consequences of varying this distance have been shown to be minor.[32] A similar diffusion zone will occur on the corroding steel surface as indicated by the narrow light blue zone at this surface in Figure 2. However, this zone is expected to be effectively nonexistent because the anticipated corrosion rate of steel (~0.1 μm/year) will be many orders of magnitude greater than that of the fuel.[24] The $[H_2]$ and $[Fe^{2+}]$ are uniform in the bulk solution (i.e., beyond the diffusion zones) and are assumed to depend on the corrosion behavior of the steel vessel. The concentrations of all radiolytic species and fuel corrosion products are assumed to be zero in the bulk solution beyond the diffusion zone. The average alpha dose rate used in all calculations is 9.03×10^5 Gy a^{-1}, (Gy a^{-1}: the absorption of one joule of radiation energy per kilogram of matter per year), corresponding to CANDU fuel, with a burn-up of 220 MWh kg U^{-1} at 1000 years after discharge from reactor.[33]

The mathematical model is numerically solved using COMSOL Multiphysics based on the finite element method. The model was simulated using the chemical engineering and the dilute species transport modules (version 4.3.0.151, COMSOL Inc.). Because the groundwater between the two corrosion fronts is stagnant and contains an excess of inert ions, e.g., Na^+ and Cl^-, the rates of the various processes in the model can be considered governed by a series of diffusion-reaction equations without convection and migration. The values of the parameters used in calculations have been listed[23] and discussed in detail elsewhere.[22,23,32] Except in the case of the parameters discussed below, these previously listed values are used in all calculations.

Reaction 3c (Figure 1), the reduction of adsorbed UO_2^{2+} by H_2 catalyzed on the surface of noble metal particles, has been studied by Nilsson et al.[29] Based on experiments using Pd (to simulate noble metal particles) in an aqueous UO_2^{2+} solution with a H_2 atmosphere, it is claimed that the reaction rate is independent of the dissolved $[H_2]$ when the H_2 pressure is varied between 1.5 and 40 bar and can be represented by the rate eq 1, in which s_ε is the fractional surface coverage by ε-particles (taken to 0.01) and k_{3c} is the rate constant measured to be 1.5×10^{-5} m s^{-1}.[29]

$$R_{3c} = k_{3c}[UO_2^{2+}]s_\varepsilon \quad (1)$$

The lowest $[H_2]$ used in this study was 1.17×10^{-3} M (the solubility at a pressure of 1.5 bar). However, fuel corrosion kinetics are expected to be influenced by $[H_2]$ at much lower $[H_2]$. It is reasonable to assume that for a bimolecular process, the reaction kinetics would eventually depend on both $[H_2]$ and $[UO_2^{2+}]$. A total of three possible scenarios are plotted in different colors in Figure 3 showing how the kinetics of reaction

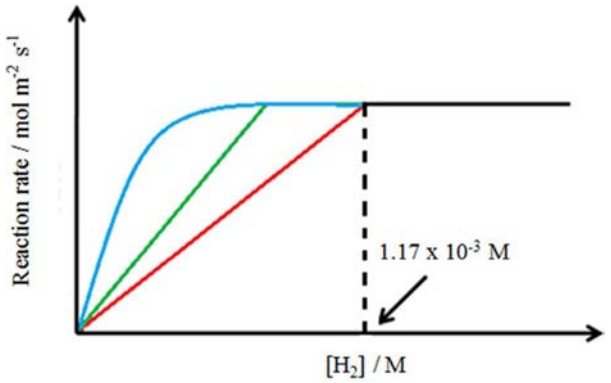

Figure 3. A total of three possible scenarios for the transition in reaction kinetics for reaction 3c when $[H_2]$ approaches zero. The dashed line shows the lower bound of experimental measurements (1.17×10^{-3} M), above which the reaction rate is independent of $[H_2]$.

3c could change as the $[H_2]$ approaches zero: (1, red) the reaction could become first order with respect to H_2 immediately after the $[H_2]$ falls below the minimum concentration (1.17×10^{-3} M) used in the published measurements; (2, green) the reaction could remain independent of $[H_2]$ to lower concentrations before becoming first order; and (3, blue) the rate could change nonlinearly with $[H_2]$. It is assumed the reaction kinetics become first order with respect to both H_2 and UO_2^{2+}, as indicated in the rate in eq 2,

$$R_{3c} = k'_{3c}[UO_2^{2+}][H_2]s_\varepsilon \quad (2)$$

At low $[H_2]$ concentrations, this reaction will be controlled by the kinetics of the cathodic reaction. Because the reaction proceeds via H atoms formed on ε-particle surfaces, the use of this rate equation is equivalent to assuming that the coverage of the particle surfaces by H atoms is directly proportional to the $[H_2]$ in the solution. The rapid dissociation of H_2 required to

DOI: 10.1021/acs.est.6b04167
Environ. Sci. Technol. 2016, 50, 12348–12355

validate this assumption is expected because the particles have high Ru, Rh, and Pd contents, all metals with high exchange-current densities for the H^+-H-H_2 reaction.[34]

To use the rate in eq 2, it is necessary to specify a value for the rate constant that has not been measured. In the model presented here, the first scenario (red in Figure 3) is adopted with the slope of the red line yielding a rate constant of $k'_{3c} = 1.3 \times 10^{-5}$ [m^4 s^{-1} mol^{-1}]. This scenario is conservative from the perspective of fuel corrosion because the other two scenarios would yield larger rate constants, which would lead to faster reduction of UO_2^{2+}.

A similar approach has been adopted in selecting the rate constant for the reduction of H_2O_2 by H_2 catalyzed on noble metal particles (reaction 5 in Figure 1), the rate of which has been shown to be independent of [H_2] over the pressure range 1 to 40 bar.[31] This leads to a modified reaction rate constant, $k'_5 = 2.8 \times 10^{-5}$ [m^4 s^{-1} mol^{-1}].

3. RESULTS AND DISCUSSION

3.1. Critical Hydrogen Concentration ($[H_2]_{crit}$). *3.1.1. Influence of the Decomposition Ratio of H_2O_2 (Reaction 6, Figure 1).* The critical [H_2] ($[H_2]_{crit}$) is defined as the minimum $[H_2]_{bulk}$ required to completely suppress fuel corrosion when the [UO_2^{2+}] becomes zero. Reaction 6 (Figure 1), the decomposition of H_2O_2 to O_2 and H_2O, is expected to exert a major influence on fuel. While O_2 is also a potential fuel oxidant, the rate constant for its reaction with UO_2 is ~200 times lower than that of H_2O_2.[7,8] Calculations suggest the inclusion of reactions involving O_2 have no significant additional effect on fuel corrosion,[22] although this effect remains to be investigated in more detail. Although fuel-surface-catalyzed H_2O_2 decomposition has been observed, no detailed kinetic analysis is presently available. Based on electrochemical measurements, Wu et al.[35] demonstrated that H_2O_2 decomposition and UO_2 dissolution occur simultaneously and that decomposition could be the primary reaction pathway. These results are consistent with those of Pehrman et al.[26] who showed that surface-catalyzed decomposition accounted for 86% of the consumed H_2O_2 on UO_2 and 99.8% on a SIMFUEL pellet. Because the characteristics of the SIMFUEL were not specified in this study,[26] we have adopted the value of 86% as the fraction of H_2O_2 uninvolved in fuel corrosion due to decomposition.

Figure 4 shows this reaction has a significant influence on $[H_2]_{crit}$, especially within a 9 mm deep fracture the demand for H_2 doubling when the decomposition ratio is decreased from the adopted default value to 0.2. This is not unexpected because undecomposed H_2O_2 at deep fracture locations will make the redox conditions considerably more oxidizing, thereby increasing the demand for H_2 to suppress corrosion.

3.1.2. Influence of Fracture Geometry. Figure 5 shows the $[H_2]_{crit}$ calculated for a range of fracture dimensions using the adopted rate constants and the fractional value for H_2O_2 decomposition. For wide fractures (i.e., with a width >0.6 mm), $[H_2]_{crit}$ increases as the fracture depth increases. However, for narrow fractures (width <0.6 mm) $[H_2]_{crit}$ first increases then decreases as the fracture deepens, suggesting a significant suppression of fuel corrosion by the local accumulation of radiolytically produced H_2, $(H_2)_{int}$. This hypothesis is supported by experiments performed on UO_2 in α-irradiated distilled water, either open to or closed from the open atmosphere.[36] In the experiments, radiolytic H_2 was allowed to escape from the open system but to accumulate in the closed one. In the closed system, the dissolved U concentration was suppressed to about one-third of that observed in the open system due to the accumulation of radiolytical H_2.

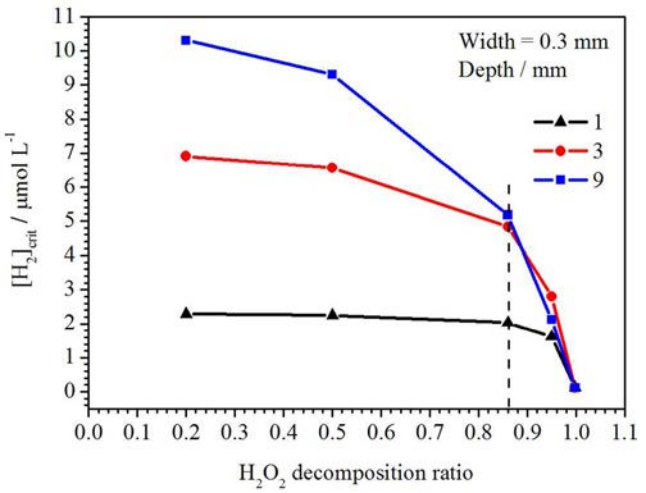

Figure 4. Critical [H_2] ($[H_2]_{crit}$) as a function of the H_2O_2 decomposition ratio and the depth of the fracture (fracture width of 0.3 mm). All other model parameters have the default values. The vertical dashed line shows the default value for the ratio.

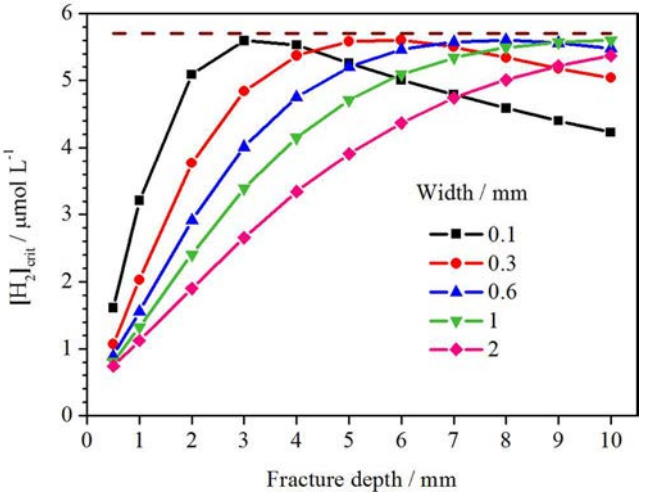

Figure 5. Critical [H_2] ($[H_2]_{crit}$) in fractures with different widths and depths for CANDU spent fuel with a burn-up of 220 MWh kg U^{1-} at 1000 years after discharge from reactor. The dashed line indicates an upper limit, 5.7 μmol L^{-1}, for the $[H_2]_{crit}$. All other model parameters have the default values.

Figure 5 suggests the existence of an upper limit (5.7 μmol L^{-1}, as indicated by the horizontal dashed line) for the $[H_2]_{crit}$ for the anticipated range of possible fracture geometries. This value is ~17 times the $[H_2]_{crit}$ required on the planar unfractured surface (~0.33 μmol L^{-1}). This upper limiting value suggests that, if the corrosion of the carbon steel canister can produce a $[H_2]_{bulk}$ > 5.7 μmol L^{-1}, the corrosion of CANDU spent fuel with the reference burn-up level of 220 MWh kg U^{-1} should be completely suppressed.

3.2. Separation of the Effects of Internal and External H_2 on the Corrosion of a Fracture Wall. The plots in Figure 5 indicate a significant role for $[H_2]_{int}$ in the suppression of corrosion in narrow and deep fracture locations. This offers the

DOI: 10.1021/acs.est.6b04167
Environ. Sci. Technol. 2016, 50, 12348−12355

prospect that the demand for $(H_2)_{ext}$ will be considerably lower than expected, and the limitations on its transport to these deep locations will not prevent the suppression of fuel corrosion. The separation of the influences of $(H_2)_{int}$ and $(H_2)_{ext}$ is experimentally extremely difficult but can be investigated via modeling.

Figure 6 shows the individual and combined influences of $(H_2)_{int}$ and $(H_2)_{ext}$ on the corrosion of the walls of a narrow and relatively deep fracture (width = 0.3 mm, depth = 6 mm). As expected, the combined influence leads to a lower corrosion rate)Figure 6A), the flux difference between the black ($(H_2)_{int}$ + $(H_2)_{ext}$) and orange ($(H_2)_{ext}$ only) lines defining the effect of $(H_2)_{int}$ (shown in green in Figure 6 A) on the corrosion rate. Similarly, the difference between the red ($(H_2)_{int}$ only) and black ($(H_2)_{int}$ + $(H_2)_{ext}$) lines defines the influence of $(H_2)_{ext}$ (shown in blue in Figure 6B).

Because the separate H_2 effects on the corrosion rate should be proportional to their respective concentrations, the ratio of $[H_2]_{int}$ to the $[H_2]_{total}$ (total of $(H_2)_{int}$ + $(H_2)_{ext}$) along the wall of the fracture defines the fractional influence of $(H_2)_{int}$. Similarly, the ratio $[H_2]_{ext}$-to-$[H_2]_{total}$ ratio along the wall of the fracture defines the fractional influence of $(H_2)_{ext}$. These fractions are plotted in Figure 6C. These calculations demonstrate that the effects of $(H_2)_{int}$ and $(H_2)_{ext}$ can be modeled via either the flux difference or the ratio of their respective concentrations at a specific location. In the calculations below, the effects are simulated by comparing the respective concentrations.

Fuel corrosion cannot be totally suppressed with only internal H_2 for both planar and fractured spent fuel with the dose rate of 9.03×10^5 Gy.a^{-1}. For a planar fuel surface, when the corrosion of carbon steel could sustain $[H_2]_{bulk} \geq 0.33$ μM (the $[H_2]_{crit}$), with the help of external H_2, the fuel corrosion can be totally suppressed. When we set the $[H_2]_{bulk} = 0.1$ μM, the internal H_2 takes only 8.7% of the responsibility in suppressing fuel corrosion. For a fractured spent fuel (width = 0.3 mm, depth =6 mm), when the corrosion of carbon steel could sustain $[H_2]_{bulk} \geq 5.60$ μM (the $[H_2]_{crit}$), the fuel corrosion can be totally suppressed. When we set the $[H_2]_{bulk}$ = 0.1 μM, the internal H_2 takes ~94% of the responsibility in suppressing fuel corrosion at the bottom of the fracture and ~60% at the mouth of the fracture (Figure 6C). The comparison shows the fractured spent fuel needs a higher $[H_2]_{bulk}$ to totally suppress fuel corrosion, and internal H_2 plays a much more important role of suppressing corrosion for the fractured fuel surface than it does on a planar surface.

3.2.1. Influence of Fracture Depth. Figure 7A shows the concentration profiles for $(H_2)_{int}$ for fractures with different depths (0.5, 1, 3, and 6 mm) and a constant width (0.6 mm). As the fracture becomes deeper, $(H_2)_{int}$ accumulates at the bottom of the fracture as its loss by diffusion out of the fracture becomes limited. Figure 7B shows the fractions of $(H_2)_{int}$ and $(H_2)_{ext}$ used in suppressing corrosion as a function of the normalized distance from the base of fractures of various depths. In this case, the bulk $[H_2]$ (supplied by steel canister corrosion) is low (10^{-8} M), and the fuel has a relatively high dose rate (9.03×10^5 Gy a^{-1}) (producing radiolytic H_2). Thus, for the geometries tested, the radiolytic H_2 ($(H_2)_{int}$) is always more important than H_2 from steel corrosion ($(H_2)_{ext}$. As the fracture becomes deeper the influence of $(H_2)_{int}$ in suppressing corrosion of the walls of the fracture becomes dominant increasing from ~70% (0.5 mm depth) to ~98% (6 mm depth).

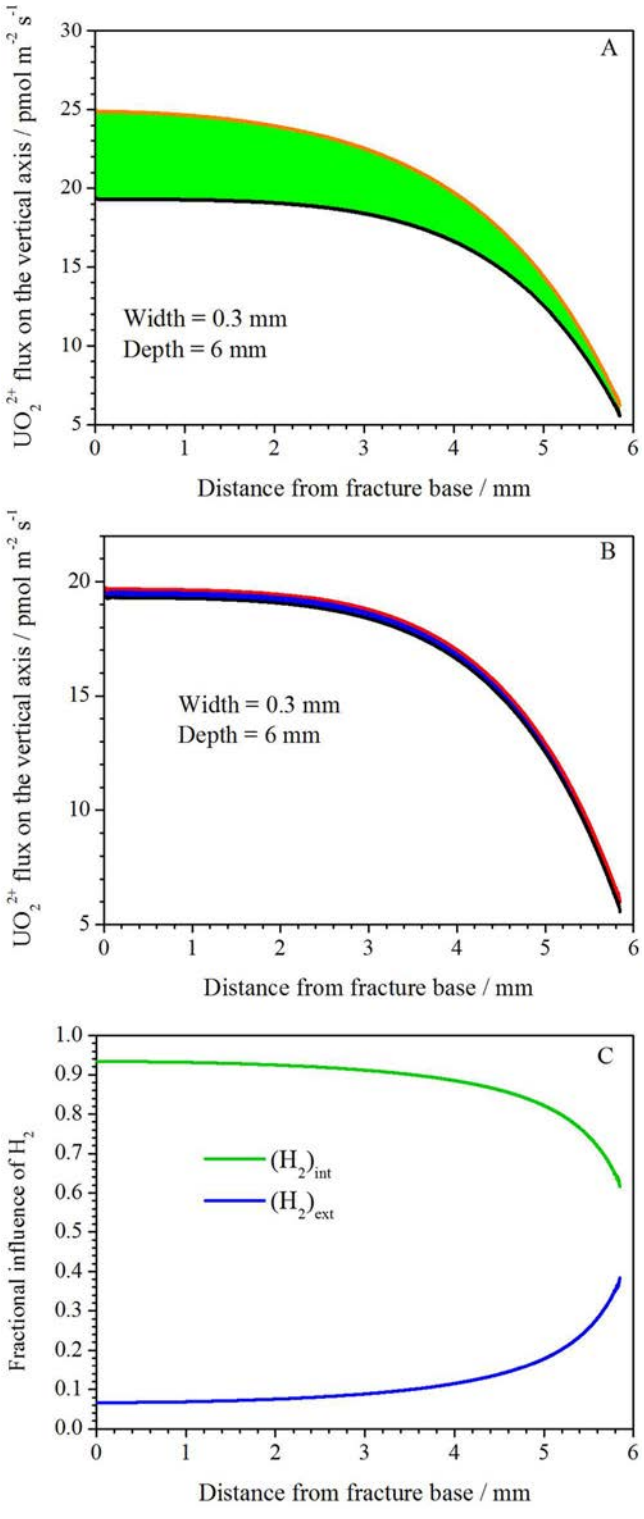

Figure 6. (A,B) The calculated flux of UO_2^{2+} (equivalent to fuel corrosion rate) in the direction normal to the wall of a narrow and deep fracture as a function of the distance from the base of the fracture. The black lines in A and B indicate the calculated UO_2^{2+} flux with both $(H_2)_{int}$ and $(H_2)_{ext}$; the orange line in A indicates the UO_2^{2+} flux with only $(H_2)_{ext}$; the red line in B indicates the UO_2^{2+} flux with only $(H_2)_{int}$. (C) The calculated fractional influence of H_2 from both sources based on a comparison of the respective concentrations. Fracture depth = 6 mm; fracture width = 0.3 mm; $[H_2]_{bulk} = 10^{-7}$ M. All other model parameters have their default values.

DOI: 10.1021/acs.est.6b04167
Environ. Sci. Technol. 2016, 50, 12348−12355

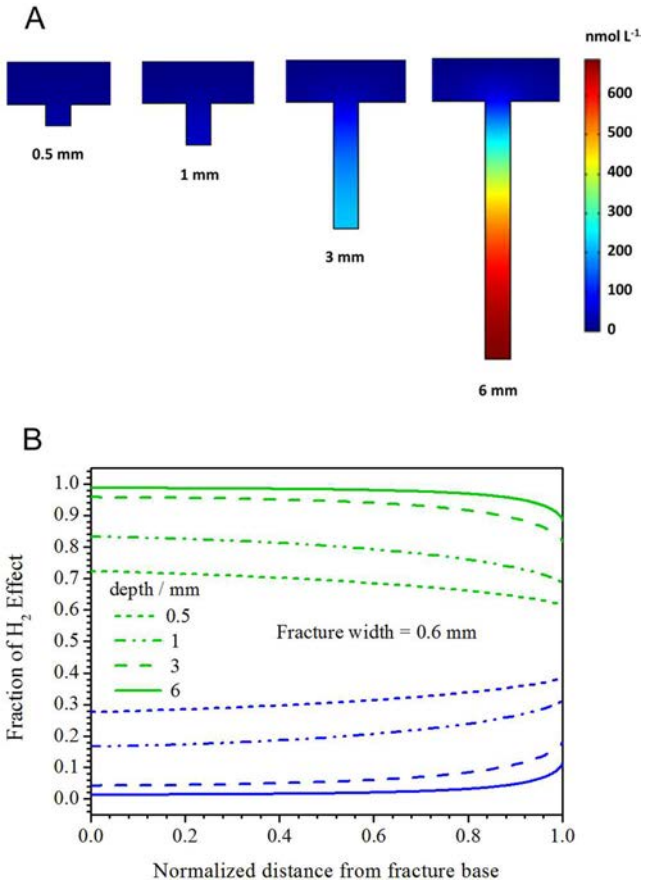

Figure 7. Concentration profiles for $(H_2)_{int}$ (A) and the fractional influences of $(H_2)_{int}$ (green) and $(H_2)_{ext}$ (blue) (B) in fractures with different depths (0.5, 1, 3, and 6 mm) and a constant width (0.6 mm). $[H_2]_{bulk} = 10^{-8}$ M; all other model parameters have the default values. A schematic description of the fracture is shown in Figure 2.

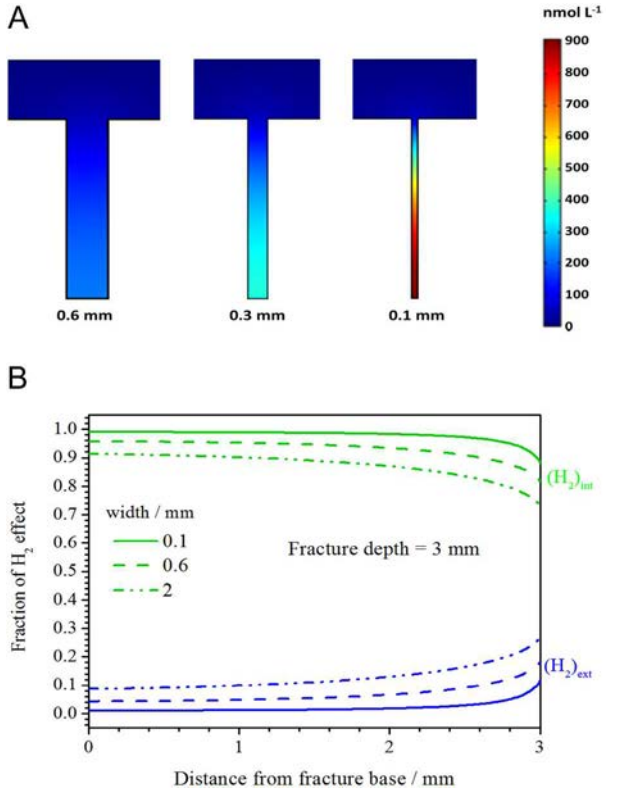

Figure 8. Concentration profiles for $(H_2)_{int}$ (A) and the fractional influences of $(H_2)_{int}$ (green) and $(H_2)_{ext}$ (blue) (B) in fractures with different widths (0.1, 0.3, and 0.6 mm) and a constant depth (3 mm); $[H_2]_{bulk} = 10^{-8}$ M; all other model parameters have the default values. A schematic description of the fracture is shown in Figure 2.

3.2.2. Influence of the Fracture Width. Figure 8A shows the concentration profiles of $(H_2)_{int}$ for fractures with different widths (0.6, 0.3, and 0.1 mm) and a constant depth (3 mm). As the fracture gets narrower, there is a greater accumulation of the $(H_2)_{int}$ within the fracture, resulting in an increasing fraction of the $(H_2)_{int}$ effect as shown in Figure 8B.

The importance of the fractures is that they can act as locations at which H_2O_2 and H_2, produced by the α-radiolysis of H_2O, can accumulate and be partially isolated from the redox scavengers (H_2 and Fe^{2+}) produced by corrosion of the steel vessel, leading to an increase or decrease in fuel corrosion rate, depending on the fracture geometry.

A number of reactions have been shown able to moderate the influence of H_2O_2 leading to a reduction in corrosion rate. These include the surface-catalyzed decomposition of H_2O_2 to H_2O and the much-less-reactive oxidant, O_2 and a number of reactions involving H_2 (produced either by α-radiolysis or by corrosion of the steel vessel), which can both directly suppress the corrosion of UO_2 and consume H_2O_2 in reactions catalyzed on the noble metal particles present in the fuel matrix.

The catalytic decomposition of H_2O_2 has been shown to be a key reaction in moderating the corrosion of the fuel, although a fully developed kinetic model is not presently available. For the remaining undecomposed H_2O_2, the model suggests that, for CANDU fuel with moderate in-reactor burn-up, only micromolar concentrations of dissolved H_2 are required to completely suppress fuel corrosion and that, even within deep fractures in the fuel, the "demand" for H_2 is only approximately 17 times that required on the outer planar surface of the fuel.

By the separation of the influences on corrosion of radiolytic H_2 ($(H_2)_{int}$) and H_2 from steel corrosion ($(H_2)_{ext}$), the model shows their relative influence is strongly affected by the dimensions of fractures in the fuel and by the amount of H_2 produced by corrosion. If only small amounts of H_2 are produced by steel corrosion, then radiolytic H_2 exerts the dominant influence on fuel corrosion because the transport of $(H_2)_{int}$ out of the fracture is limited, especially if it is deep and narrow. Even when larger amounts of H_2 are produced by steel corrosion, radiolytic H_2 remains the dominant reductant, suppressing fuel corrosion in deep narrow fractures.

A number of mechanistic details and kinetic deficiencies remain unresolved. The kinetics of reactions involving H_2, H_2, and H_2O_2 and the decomposition of H_2O_2 (to O_2 and H_2O) are not known within the concentration ranges important for spent nuclear fuel. Although these deficiencies may be covered by conservative assumptions in the calculations presented, they preclude any attempts to validate the model.

■ ASSOCIATED CONTENT

Supporting Information

The Supporting Information is available free of charge on the ACS Publications website at DOI: 10.1021/acs.est.6b04167.

Additional details on the influence of the adoption of the modified rate constants (k'_{3c} and k'_{5}) on the critical $[H_2]$, the influence of time on the critical $[H_2]$ since

DOI: 10.1021/acs.est.6b04167
Environ. Sci. Technol. 2016, 50, 12348−12355

emplacement in the repository, the influence of the $[H_2]_{bulk}$, and the α dose rate on the separation of the $(H_2)_{int}$ and $(H_2)_{ext}$ effect on the wall of a fracture. The separation of the $(H_2)_{int}$ and $(H_2)_{ext}$ effect at the base of a fracture. Figures showing the critical $[H_2]$ ($[H_2]_{crit}$) as a function of the rate constant (k'_5) for reaction 5, the critical $[H_2]$ ($[H_2]_{crit}$) as a function of time since emplacement in a repository, the fractional influences of $(H_2)_{ext}$ for different $[H_2]_{bulk}$, The UO_2^{2+} flux at the bottom of a fracture as a function of fracture depth, and the UO_2^{2+} flux at the base of a fracture as a function of the $[H_2]_{bulk}$. (PDF)

AUTHOR INFORMATION

Corresponding Author

*Phone: 519-661-2111 (nos. 86366 and 86154); fax: 519-661-3022; e-mail: dwshoesm@uwo.ca.

Notes

The authors declare no competing financial interest.

ACKNOWLEDGMENTS

This research was funded under the Industrial Research Chair agreement between the Natural Science and Engineering Research Council (NSERC, Ottawa) and the Nuclear Waste Management Organization (NWMO, Toronto).

REFERENCES

(1) NWMO. *Implementing adaptive phased management 2016 to 2020*; Nuclear Waste Management Organization: Toronto, Ontario, 2016; http://www.nwmo.ca.

(2) McMurry, J.; Dixon, D. A.; Garroni, J. D.; Ikeda, B. M.; Stroes-Gascoyne, S.; Baumgartner, P.; Melnyk, T. W. *Evolution of a Canadian Deep Geologic Repository: Base Scenario*; Report 06819-REP-01200−10092-R00; Ontario Power Generation: Toronto, 2003.

(3) Ewing, R. C. Long-term storage of spent nuclear fuel. *Nat. Mater.* **2015**, *14*, 252−257.

(4) Shoesmith, D. W.; King, F.; Ikeda, B. M. An assessment of the feasibility of indefinite containment of Canadian nuclear fuel wastes. *AECL-10972 COG* **1995**, 94−534.

(5) King, F.; Kolar, M. *The Copper Container Corrosion Model Used in AECL's Second Case Study*; Report 06819-REP-01200−10041-R00; Ontario Power Generation: Toronto, Ontario, 2000.

(6) King, F.; Ahonen, L.; Taxén, C.; Vuorinen, U.; Werme, L. *Copper Corrosion under Expected Conditions in a Deep Geologic Repository*; Technical Report TR-01−23; Swedish Nuclear Fuel and Waste Management Co: Stockholm, 2001.

(7) Ekeroth, E.; Roth, O.; Jonsson, M. The relative impact of radiolysis products in radiation induced oxidative dissolution of UO_2. *J. Nucl. Mater.* **2006**, *355* (1−3), 38−46.

(8) Shoesmith, D. W. Fuel corrosion processes under waste disposal conditions. *J. Nucl. Mater.* **2000**, *282*, 1−31.

(9) Gu, B.; Liang, L.; Dickey, M. J.; Yin, X.; Dai, S. Reductive precipitation of Uranium(VI) by zero-valent Iron. *Environ. Sci. Technol.* **1998**, *32*, 3366−3373.

(10) Fiedor, J. N.; Bostick, W. D.; Jarabek, R. J.; Farrell, J. Understanding the mechanism of uranium removal from groundwater by zero-valent Iron using X-ray photoelectron spectroscopy. *Environ. Sci. Technol.* **1998**, *32*, 1466−1473.

(11) Rollin, S.; Spahiu, K.; Eklund, U.-B. Determination of dissolution rates of spent fuel in carbonate solutions under different redox conditions with a flow-through experiment. *J. Nucl. Mater.* **2001**, *297*, 231−243.

(12) Carbol, P.; Cobos-Sabate, J.; Glatz, J-P; Ronchi, C.; Rondinella, V.; Wegen, D. H.; Wiss, T.; Loida, A.; Metz, V.; Kienzler, B.; Spahiu, K.; Grambow, B.; Quiñones, J.; Martinez Esparza Valiente, A. *The Effect of Dissolved Hydrogen on the Dissolution of ^{233}U Doped UO_2(s), High Burn-up Spent Fuel and MOX Fuel*; Technical Report TR-05−09; Swedish Nuclear Fuel and Waste Management: Stockholm, Sweden, 2005.

(13) Cui, D.; Low, J.; Spahiu, K. Environmental behaviors of spent nuclear fuel and canister materials. *Energy Environ. Sci.* **2011**, *4*, 2537−2545.

(14) Shoesmith, D. W. *The Role of Dissolved Hydrogen on the Corrosion/Dissolution of Spent Nuclear Fuel*; Report NWMO TR-2008−19; Nuclear Waste Management Organization: Toronto, 2008.

(15) Broczkowski, M. E.; Keech, P. G.; Noël, J. J.; Shoesmith, D. W. Corrosion of uranium dioxide containing simulated fission products in dilute hydrogen peroxide and dissolved hydrogen. *J. Electrochem. Soc.* **2010**, *157* (8), C275−C281.

(16) Broczkowski, M. E.; Noël, J. J.; Shoesmith, D. W. The inhibiting effects of hydrogen on the corrosion of uranium dioxide under nuclear waste disposal conditions. *J. Nucl. Mater.* **2005**, *346* (1), 16−23.

(17) Broczkowski, M. E.; Noël, J. J.; Shoesmith, D. W. The influence of dissolved hydrogen on the surface composition of doped uranium dioxide under aqueous corrosion conditions. *J. Electroanal. Chem.* **2007**, *602* (1), 8−16.

(18) Trummer, M.; Roth, O.; Jonsson, M. H_2 inhibition of radiation induced dissolution of spent nuclear fuel. *J. Nucl. Mater.* **2009**, *383* (3), 226−230.

(19) Eriksen, T. E.; Shoesmith, D. W.; Jonsson, M. Radiation induced dissolution of UO_2 based nuclear fuel − A critical review of predictive modelling approaches. *J. Nucl. Mater.* **2012**, *420* (1−3), 409−423.

(20) Shoesmith, D. W.; Kolar, M.; King, F. A mixed-potential model to predict fuel (uranium dioxide) corrosion within a failed nuclear waste container. *Corrosion* **2003**, *59* (9), 802−815.

(21) Jonsson, M.; Nielsen, F.; Roth, O.; Ekeroth, E.; Nilsson, S.; Hossain, M. M. Radiation induced spent nuclear fuel dissolution under deep repository conditions. *Environ. Sci. Technol.* **2007**, *41*, 7087−7093.

(22) Wu, L.; Qin, Z.; Shoesmith, D. W. An improved model for the corrosion of used nuclear fuel inside a failed waste container under permanent disposal conditions. *Corros. Sci.* **2014**, *84*, 85−95.

(23) Wu, L.; Liu, N.; Qin, Z.; Shoesmith, D. W. Modeling the radiolytic corrosion of fractured nuclear fuel under permanent disposal conditions. *J. Electrochem. Soc.* **2014**, *161* (8), E3259−E3266.

(24) Hill, S. L. W.; Liu, N.; Qin, Z.; Zagidulin, D.; Shoesmith, D. W. Interactions between carbon steel and UO_2 corrosion fronts inside a failed nuclear waste container. *Proceedings of the 17th International Conference on Environmental Degradation of Materials in Nuclear Power Systems − Water Reactors*; Ottawa, Ontario, August 9−13, 2015; Canadian Nuclear Society (CNS): Toronto, 2015.

(25) Shoesmith, D. W. *Used fuel and uranium dioxide dissolution studies − A review*; Report NWMO TR-2007−03; Nuclear Waste Management Organization: Toronto, Ontario, 2007.

(26) Pehrman, R.; Trummer, M.; Lousada, C. M.; Jonsson, M. On the redox reactivity of doped UO_2 pellets − Influence of dopants on the H_2O_2 decomposition mechanism. *J. Nucl. Mater.* **2012**, *430* (1−3), 6−11.

(27) Trummer, M.; Nilsson, S.; Jonsson, M. On the effects of fission product noble metal inclusions on the kinetics of radiation induced dissolution of spent nuclear fuel. *J. Nucl. Mater.* **2008**, *378* (1), 55−59.

(28) Ekeroth, E.; Jonsson, M.; Eriksen, T. E.; Ljungqvist, K.; Kovács, S.; Puigdomenech, I. Reduction of UO_2^{2+} by H_2. *J. Nucl. Mater.* **2004**, *334* (1), 35−39.

(29) Nilsson, S.; Jonsson, M. On the catalytic effect of Pd(s) on the reduction of UO_2^{2+} with H_2 in aqueous solution. *J. Nucl. Mater.* **2008**, *374* (1−2), 290−292.

(30) Millero, F. J.; Sotolongo, S. The oxidation of Fe (II) with H_2O_2 in seawater. *Geochim. Cosmochim. Acta* **1989**, *53*, 1867−1873.

(31) Nilsson, S.; Jonsson, M. On the catalytic effects of UO_2(s) and Pd(s) on the reaction between H_2O_2 and H_2 in aqueous solution. *J. Nucl. Mater.* **2008**, *372* (2−3), 160−163.

(32) Wu, L.; Beauregard, Y.; Qin, Z.; Rohani, S.; Shoesmith, D. W. A model for the influence of steel corrosion products on nuclear fuel

DOI: 10.1021/acs.est.6b04167
Environ. Sci. Technol. 2016, 50, 12348−12355

corrosion under permanent disposal conditions. *Corros. Sci.* **2012**, *61*, 83−91.
(33) Garisto, F.; Barber, D. H.; Chen, E.; Inglot, A.; Morrison, C. A. *Alpha, beta and gamma dose rates in water in contact with used CANDU Fuel*; Report NWMO TR-2009−27; Nuclear Waste Management Organization: Toronto, Ontario, 2009.
(34) Norskov, J. K.; Bligaard, T.; Logadottir, A.; Kitchin, J. R.; Chen, J. G.; Pandelov, S.; Stimming, U. Trends in the Exchange Current for Hydrogen Evolution. *J. Electrochem. Soc.* **2005**, *152*, J23−J26.
(35) Wu, L.; Shoesmith, D. W. An electrochemical study of H_2O_2 oxidation and decomposition on simulated nuclear fuel (SIMFUEL). *Electrochim. Acta* **2014**, *137*, 83−90.
(36) Traboulsi, A.; Vandenborre, J.; Blain, G.; Humbert, B.; Barbet, J.; Fattahi, M. Radiolytic corrosion of uranium dioxide: role of molecular species. *J. Phys. Chem. C* **2014**, *118* (2), 1071−1080.

DOI: 10.1021/acs.est.6b04167
Environ. Sci. Technol. 2016, 50, 12348−12355